A novel joint support vector machine-cubature Kalman filtering method for adaptive state of charge prediction of lithium-ion batteries.

SONG, Q., WANG, S., XU, W., SHAO, Y. and FERNANDEZ, C.

2021

Int. J. Electrochem. Sci., 16 **(2021)** Article ID: 210823, doi: 10.20964/2021.08.26

International Journal of
ELECTROCHEMICAL
SCIENCE
www.electrochemsci.org

A Novel Joint Support Vector Machine - Cubature Kalman Filtering Method for Adaptive State of Charge Prediction of Lithium-Ion Batteries

Qianqian Song[1], *Shunli Wang*[1,*], *Wenhua Xu*[1], *Yanhua Shao*[1], *Carlos Fernandez*[2]

[1] School of Information Engineering, Southwest University of Science and Technology, Mianyang 621010, China;
[2] School of +Pharmacy and Life Sciences, Robert Gordon University, Aberdeen AB10-7GJ, UK.
[*]E-mail: wangshunli@swust.edu.cn

Received: 11 April 2021 / *Accepted:* 1 June 2021 / *Published:* 30 June 2021

Accurate estimation of SOC of lithium-ion batteries has always been an important work in the battery management system. However, it is often very difficult to accurately estimate the SOC of lithium-ion batteries. Therefore, a novel joint support vector machine - cubature Kalman filtering (SVM-CKF) method is proposed in this paper. SVM is used to train the output data of the CKF algorithm to obtain the model. Meanwhile, the output data of the model is used to compensate the original SOC, to obtain a more accurate estimate of SOC. After the SVM-CKF algorithm is introduced, the amount of data needed for prediction is reduced. By using Beijing Bus Dynamic Stress Test (BBDST) and the Dynamic Stress Test (DST) condition to verify the training model, the results show that the SVM-CKF algorithm can significantly improve the estimation accuracy of Lithium-ion battery SOC, and the maximum error of SOC prediction for BBDST condition is 0.800%, which is reduced by 0.500% compared with CKF algorithm. The maximum error of SOC prediction under DST condition is about 0.450%, which is 1.350% less than that of the CKF algorithm. The overall algorithm has a great improvement in generalization ability, which lays a foundation for subsequent research on SOC prediction.

Keywords: lithium-ion battery; Thevenin model; state of charge; support vector machine; cubature Kalman filter

1. INTRODUCTION

In the 21st century, the energy problem has become one of the great challenges for us human beings. Such a large amount of energy consumption is bound to bring about a more serious greenhouse effect [1], global warming [2, 3], rising sea levels [4], and so on. On the other hand, with the growth of the world's population [5], the energy consumption of the world is bound to increase substantially, so it is particularly important to seek new energy to replace the fossil energy. As a new type of clean energy

[6], Lithium-ion batteries have the advantages of high storage energy density [7], long service life [8], and lightweight. They are bound to play a major role now and in the future.

With the widespread use of Lithium-ion batteries, people are increasingly concerned about the remaining useful life(RUL) [9, 10], battery life, the prediction of capacity [11], the state of health(SOH) [12-14], and safety [15]of Lithium-ion batteries. One of the most important is the accurate estimation of the state of charge (SOC) [16-18] of the Lithium-ion battery. The battery's SOC reflects the battery's endurance and the real-time remaining power of the battery, which greatly affects the user's experience.

The SOC of a Lithium-ion battery is affected by current, voltage, aging, and other factors, so it is particularly difficult to estimate the SOC of a Lithium-ion battery. At present, the main methods for estimating the SOC of Lithium-ion batteries include the ampere-hour method [19, 20], the open-circuit voltage method [21, 22], the Kalman filter [23] (KF) method, and neural network (NN) [24-26] method.

In recent years, there have been more and more researches on the estimation of Lithium-ion battery SOC, which has become one of the important topics of new energy research in international society. Lots of researchers and scholars have conducted active research on the SOC of the battery, and the results are impressive. With the continuous progress of technology, researchers have put forward a lot of improved algorithms based on the former algorithm, such as the Unscented Kalman Filtering (UKF) [27, 28] algorithm, the improved Extended Kalman Filtering (EKF) algorithm [29-32] algorithm, the CKF [33, 34] and the SVM [35, 36] method. Liu et al. [37] used the unscented Kalman filter algorithm and particle filter method to predict SOC, and the results show that SOC can be predicted in real-time, and has a strong robustness to noise. He et al. [38] proposed a variable parameter equivalent hysteresis model based on the Thevenin model, which optimized the limitations of the traditional Thevenin model caused by fixed parameters. Zhu et al. [39] proposed a way to Identify model parameters Restricted Total Least Squares, which reduced the error caused by the traditional recursive least squares method due to identification error. Tian et al. [40] proposed a Long Short-Term Memory (LSTM) network combined with an Adaptive Cubature Kalman Filter (ACKF) algorithm. It can significantly improve the accuracy of SOC estimation, has excellent generalization ability for different data, and can solve the initial error.

This paper takes lithium-ion batteries as the research and modeling object. After analyzing the characteristics of lithium-ion batteries, a new method for estimating the SOC of lithium-ion batteries is proposed. The algorithm of data mining is introduced into the estimation of Lithium-ion battery SOC, and a novel joint support vector machine - cubature Kalman filtering method is proposed. This algorithm is different from the BP neural network algorithm based on the empirical risk minimization criterion, which tends to rely excessively on the training samples, while the learning convergence speed is slow, easy to fall into the local minimum, and there will be overlearning, while the SVM algorithm is based on the structural risk minimization criterion, keeps the training error fixed and minimizes the confidence range, solves the overlearning problem, and has good generalization ability to the samples. the SVM-CKF algorithm introduces the SVM algorithm based on the advantages of the CKF algorithm to improve the accuracy of the algorithm. Through the Hybrid Pulse Power Characterization (HPPC), BBDST, and DST tests, the results show that the accuracy of the algorithm for SOC estimation is effectively improved after the introduction of the SVM algorithm, which provides new ideas for future research.

2. MATHEMATICAL ANALYSIS

2.1. SVM-CKF Joint algorithm

To train and obtain an SVM model with good performance and give play to the good generalization ability of the SVM algorithm, it is necessary to select appropriate input and output. The flow chart of the joint algorithm is shown in Fig. 1.

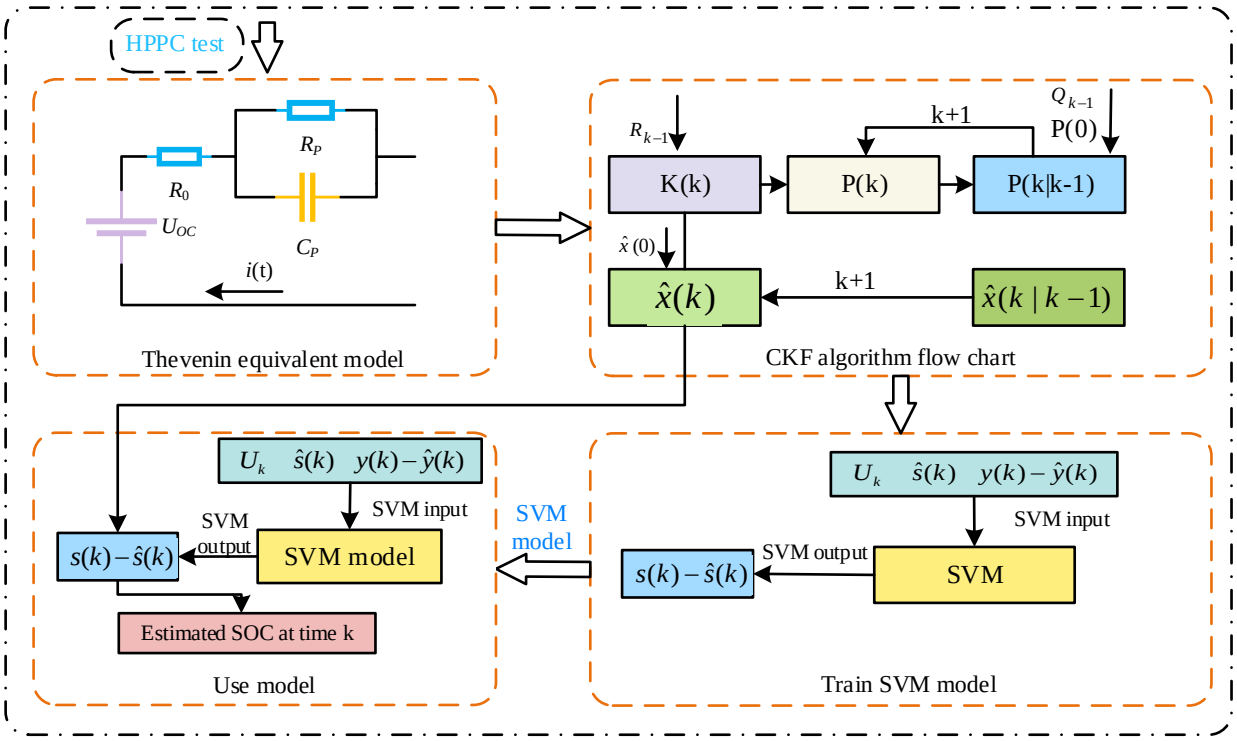

Figure 1. Joint SVM-CKF algorithm flow chart

Considering the nonlinear characteristics of the lithium-ion battery, the influence of voltage and current on the accuracy of the training model, three input and one output models were established, where the inputs are the voltage value U_k at moment k, the SOC estimate $s(k)$ of the CKF algorithm, the end voltage error $y(k) - \hat{y}(k)$ of the CKF algorithm, and the output is the estimation error $s(k) - \hat{s}(k)$. The output of the SVM can correct the SOC predicted by the CKF algorithm to make it closer to the real SOC value, giving full play to the superiority of the joint algorithm.

2.2. Battery performance model

In the process of SOC estimation of Lithium-ion battery, the biggest factor affecting its accuracy comes from the selection of Lithium-ion battery model. According to the different model building mechanisms of Lithium-ion batteries can be divided into simple chemical models, intelligent

mathematical models, and equivalent circuit models. Because the electrochemical model of Lithium-ion batteries is complex and difficult to apply, the intelligent mathematical model is theoretically possible, but the technology is difficult to achieve in the actual operation process, requiring a large amount of data for training, the time spent is relatively long, the equivalent model circuit is simple, although it does not consider the internal chemical reaction of Lithium-ion batteries, it can well show the open-circuit voltage internal resistance during the experiment, the polarization resistance. Therefore, the equivalent model is chosen in this paper. The equivalent model is divided into the Rint model, Thevenin model, and PNGV model, etc. The Rint model consists of the internal resistance of the battery and the ideal voltage source, which has a simple structure and cannot respond to the complex chemical reactions inside the Lithium-ion battery. The PNGV model consists of an ideal voltage source, capacitor, ohmic internal resistance, and an RC circuit, and the PNGV model has an additional capacitor compared with the Thevenin model, which will increase the difficulty of subsequent parameter identification. Considering the complexity of the model and the extent to which it reflects the dynamic characteristics of the Lithium-ion battery, the circuit diagram of the Thevenin model is shown in Figure .

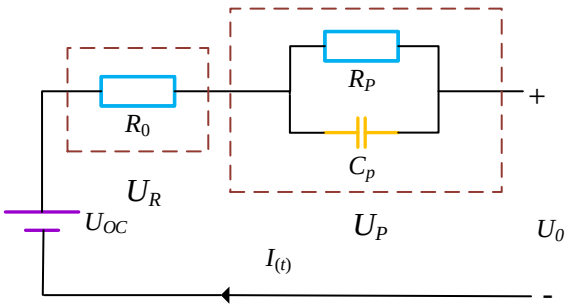

Figure 2. Thevenin equivalent circuit model

In the above circuit, R_0 can show the change of Lithium-ion battery at the instant of charging and discharging, while the RC circuit can reflect the polarization effect of the battery. the open-circuit voltage of U_{OC} cell, U_R is the voltage across the ohmic internal resistance, and U_P is the voltage division of the RC circuit, the following expression can be obtained according to Kirchhoff's law. The equivalent circuit expression can be obtained from this model as shown in Eq. (1).

$$\begin{cases} U_0 = U_{OC} - U_R - U_P \\ I(t) = C_p \dfrac{dU_p}{dt} + \dfrac{U_p}{R_p} \end{cases} \tag{1}$$

The SOC of the battery is also called the residual power, the definition of SOC is the ratio of the remaining discharged power to the rated power of the battery because the definition of SOC is too complicated to calculate SOC, so in engineering, usually use the Ampere-hour method to calculate the SOC of the battery, using the Ampere-hour method first need to know the initial value of the SOC, and then add or subtract the charge and discharge power in a period interval, to get the SOC value. The SOC value at this time is obtained, and the specific expression is shown in Eq. (2).

$$SOC_t = SOC_{t_0} - \frac{\int_{t_0}^{t} I(t)\eta dt}{Q_0} \tag{2}$$

Based on the knowledge of modern control theory, the Thevenin model of Eq. (1) and (2) is discretized. At the same time, the state space variables, input variables and output variables are selected in combination with the expression of SOC, and the following Eq. (3) can be obtained.

$$\begin{cases} \begin{bmatrix} SOC_{k+1} \\ U_{1,k+1} \end{bmatrix} = \begin{bmatrix} 1 & 0 \\ 0 & e^{-\frac{\Delta t}{\tau_1}} \end{bmatrix} \begin{bmatrix} SOC_k \\ U_{0,k+1} \end{bmatrix} + \begin{bmatrix} -\frac{\Delta t}{Q_N} \\ R_1\left(1-e^{-\frac{T}{\tau_1}}\right) \end{bmatrix} I_k + \begin{bmatrix} w_{1,k} \\ w_{2,k} \end{bmatrix} \\ U_{0,k} = U_{oc,k} - R_{0,k} I_{k+} \begin{bmatrix} 0 \\ -1 \end{bmatrix}^T \begin{bmatrix} SOC_k \\ U_{1,k} \end{bmatrix} + v_k \end{cases} \tag{3}$$

Where Δt is the time interval of sampling, τ is the time constant, and its expression is $\tau = RpCp$, ω is the state noise, while v_k is the measurement noise, and ω and ν their variances are Q_k and R_k, respectively.

2.3. Parameter identification

To complete the accurate construction of equivalent circuit modeling (EMC), it is necessary to obtain the relationship between the internal parameters of the equivalent circuit model and the SOC of the Lithium-ion battery, and the method to obtain the relationship between the internal parameters of the equivalent circuit model and the SOC of Lithium-ion battery is parameter identification.

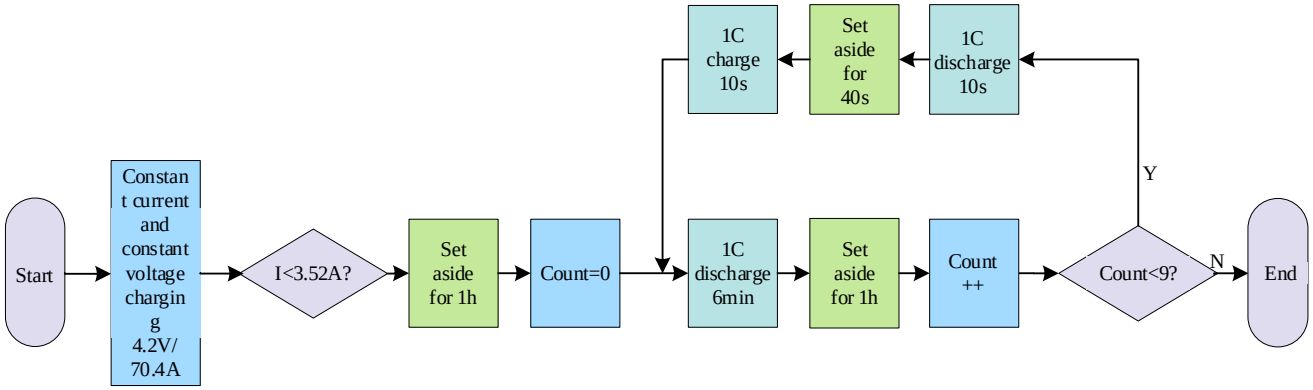

Figure 3. HPPC experimental procedure

There are two methods of parameter identification, one is online parameter identification and the other is offline parameter identification. On-line parameter identification is more complicated, and the situation of filtering saturation will occur, while off-line parameter identification is simple and easy to operate. Therefore, this paper adopts the method of off-line parameter identification, using ternary Lithium-ion battery for testing, the nominal capacity of the battery is 70Ah, after the capacity calibration

experiment, the actual capacity obtained is 70.4Ah. HPPC experiments are necessary to obtain the parameters of the Thevenin model. The experimental data for parameter identification were measured in a 25°C thermostat for the Lithium-ion battery in the HPPC experiment and the flow chart of the HPPC experiment is shown in

Figure.

In the HPPC experiment, when the SOC of the lithium-ion battery drops by 0.1, the discharge time of 10s is selected for curve fitting. According to the first-order Thevenin model, the circuit expression can be obtained from the KVL relation of the circuit in the zero-state response, and then the circuit expression is abstracted, and the parameters to be identified can be obtained according to the above expression. The above equation is shown in Eq. (2)

$$\begin{cases} U_L = U_{oc} - IR_0 - IR_P(1-e^{-\frac{x}{c}}) \\ y = a - b(1-e^{-\frac{x}{c}}) \\ R_0 = \dfrac{U_{OC} - a}{I} \\ R_P = \dfrac{b}{I} \\ C_P = \dfrac{c}{R_P} \end{cases} \tag{4}$$

2.4. Cubature Kalman Filter Algorithm

The Cubature Kalman filter algorithm uses the framework of the Unscented Kalman algorithm, the core of which is the spherical radial cubature criterion. The 2n cubature points with equal weights are selected, and then these cubature points are collectively nonlinearly transformed, and then the corresponding predicted values are obtained based on the transformed statistical characteristics. The solution process of the Cubature Kalman filter algorithm can be roughly divided into three parts, which are initialization, time update, and cubature update.

First, the parameters are initialized, this can be calculated with Eq.(5). At the same time, the initial value of measurement noise, process noise covariance, and sampling time is set. And the E (·) denotes the mathematical expectation.

$$\begin{cases} \hat{X}_0 = E\left(X_0\right) \\ P_0 = E\left(X_0 - \hat{X}_0\right)\left(X_0 - \hat{X}_0\right)^T \end{cases} \tag{5}$$

Second, time should be updated. The cubature point calculation is shown in Eq.(6), where ζ_i denotes the ith cubature point. Where n represents the estimated state dimension. The total number of cube points is twice the state dimension.

$$\begin{cases} P_{k-1} = S_{k-1}S_{k-1}^T \\ x_{k-1}^i = S_{k-1}\xi i + \hat{x}_{k-1}, i = 1, 2, \ldots 2n \end{cases} \tag{6}$$

$$\xi_i = \begin{cases} \sqrt{n}I, i = 1, 2, ...n \\ -\sqrt{n}I, i = n+1, n+2, ...2n \end{cases}$$

The propagation cubature point equation, the equations for calculating the predicted values of the state variables, and the predicted values of the error covariance are shown in Eq.(7). Where Qk is shown as the process noise covariance matrix at time k.

$$\begin{cases} x_{k|k-1}^i = f(x_{k-1}^i) \\ \hat{x}_{k|k-1} = \frac{1}{2n}\sum_{i=1}^{2n} x_{k|k-1}^i \\ P_{k|k-1} = \frac{1}{2n}\sum_{i=1}^{n}(x_{k|k-1}^i - \hat{x}_{k|k-1})(x_{k|k-1}^i - \hat{x}_{k|k-1})^T + Q_{k-1} \end{cases} \tag{7}$$

The equation to form the cubature point based on the predicted value is shown in Eq.(8). Where $\hat{x}_{k|k-1}$represents the empirical value. The accuracy of the prior value can be updated by the measurement value. And the posterior value is generated through this process.

$$\begin{cases} P_{k|k-1} = S_{k|k-1}S_{k|k-1}^T \\ x_{k|k-1}^i = S_{k|k-1}\varepsilon_i + \hat{x}_{k|k-1} \end{cases} \tag{8}$$

The equation for estimating the output of each sample point and calculating the predicted value of the observed output is shown in Eq.(9). Where the u_k is the system input at time *k-1*.

$$\begin{cases} y_{k|k-1}^i = h(x_{k|k-1}^i, u_k) \\ \hat{y}_{k|k-1} = \frac{1}{2n}\sum_{i=1}^{2n} y_{k|k-1}^i \end{cases} \tag{9}$$

The measurement covariance and cross-covariance matrices of calculated propagation are shown in Equation (10), where R_{k-1} is the measurement noise covariance matrix with time step k.

$$\begin{cases} P_{k|k-1}^z = \frac{1}{2n}\sum_{i=1}^{2n}(y_{k|k-1}^i - \hat{y}_{k|k-1})(y_{k|k-1}^i - \hat{y}_{k|k-1})^T + R_{k-1} \\ P_{k|k-1}^{xz} = \frac{1}{2n}\sum_{i=1}^{n}(x_{k|k-1}^i - \hat{x}_{k|k-1})(y_{k|k-1}^i - \hat{y}_{k|k-1})^T \end{cases} \tag{10}$$

The equation for estimating the Kalman gain and calculating the state estimate at time k and the state error covariance matrix estimate is shown in Eq. (11)

$$\begin{cases} K_k = P_{k|k-1}^{xz}(P_{k|k-1}^{xy})^{-1} \\ \hat{x}_k = \hat{x}_{k|k-1} + K_k(y_k - \hat{y}_k) \\ P_k = P_{k|k-1} - K_k P_{k|k-1}^z K_k^T \end{cases} \tag{11}$$

2.5. Support vector machine algorithm

SVM is a dichotomous model in statistical learning. By learning a hyperplane with the largest geometric interval to the training set in the feature space, the hyperplane can classify the training data with sufficient confidence. SVM can be applied to nonlinear classification by introducing kernel

techniques. For small sample data, SVM also has a more accurate prediction effect and strong model generalization ability.

The SVM sub-linear classification model can be defined as *f(x)=sign (w*x +b)*, and its training process can be equivalent to the following convex quadratic programming problem. The equations are shown in Eq.(12).

$$\begin{cases} \min_{w,b,\xi} = \frac{1}{2} \| w \|^2 + C \sum_{i=1}^{N} \xi_i \\ y_i (w \cdot x_i + b) \geq 1 - \xi_i, i = 1, 2, \cdots, N \\ \xi_i \geq 0, \mathrm{i} = 1, 2, \cdots, \ \mathrm{N} \end{cases} \tag{12}$$

Where *C* is the penalty factor. When the value *C* is large, the penalty for misclassification increases; when the value *C* is small, the penalty for misclassification decreases; *ζ* is the relaxation factor; *N* is the size of the training sample.

When an SVM is applied to a regression problem, it is called a Support Vector Regressor (SVR). The model of SVR is defined as *f(x)=w*x +b*, and the learning problem of SVR can be equivalent to the following optimization problem. Its equation is shown in Eq.(13).

$$\begin{cases} \min \frac{1}{2} \| w \|^2 + C \sum_{i=1}^{N} (\xi_i + \xi_i^*) \\ y_i - w \cdot x_i - b \leq \varepsilon + \xi_i \\ w \cdot x_i + b - y_i \leq \varepsilon + \xi_i^* \\ \xi_i, \xi_i^* \geq 0 \end{cases} \tag{13}$$

Where ζ, ζ*is the relaxation factor and is the punishment factor. To apply SVR to nonlinear problems, the Lagrange function is introduced into SVR. The SVR model after deformation and Gaussian kernel function are shown in Eq.(14).

$$\begin{cases} \mathrm{g(x)} = \sum_{i=1}^{N} (\alpha_i + \alpha_i^*) K(x, x_i) + b \\ K(x, z) = \exp(-\| x - z \|^2 \Big/ 2\sigma^2) \end{cases} \tag{14}$$

Wherein K (x, x_i) is the kernel function when K (x, x_i) is the polynomial kernel function K (x, z) = $(x*z+1)^p$, *p* is the order of the polynomial. And when K (x, x_i) is the Gaussian kernel function as shown in Eq.(14), σ is the width coefficient of the Gaussian kernel function. α_i, α_i^* is the Lagrange multiplier. When *α* is too small, the training accuracy is generally high, but the generalization ability of the time model is poor, and the phenomenon of overfitting is easy to appear. If *α* is too large, the training accuracy of the model is low. If it is too large, the training accuracy of the model is low. Considering the nonlinear characteristics of lithium-ion batteries, the kernel function used in this paper is RBF.

3. EXPERIMENTAL ANALYSIS

3.1. Test platform construction

As the research on Lithium-ion batteries continues, it is necessary to establish a complete battery management system (BMS) and a platform for conducting experiments. The experimental platform is roughly composed of four parts. The constructed platform is shown in Fig.4.

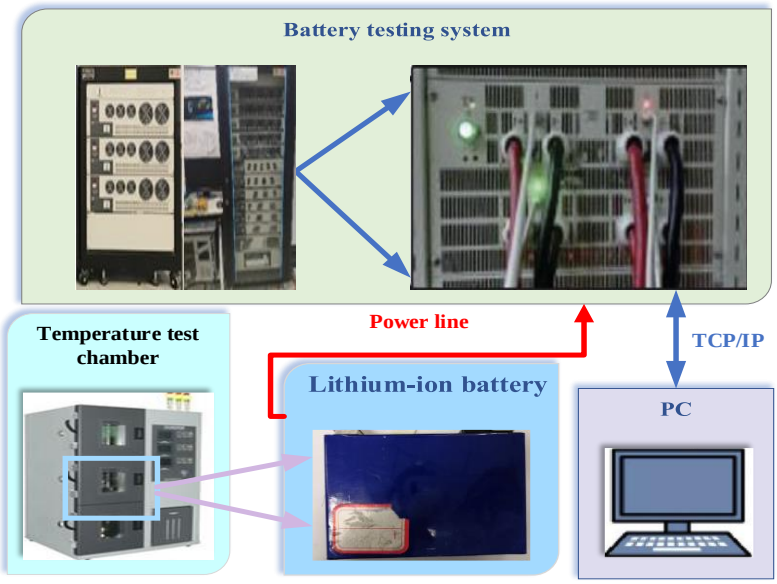

Figure 4. Test platform construction

The first part is the battery, and the ternary Lithium-ion battery is selected as the research object under the comprehensive consideration of the cost and the characteristics of the Lithium-ion battery. The second part is the computer that controls the experimental machine, which is used to set the work steps of the relevant conditions and ensure the normal conduct of the experiment. The third part is the NEWARE BTS-4000 battery testing system with 16 charging and discharging ports, which transmit the battery information to the upper computer in real-time during the testing process. The fourth part is a constant temperature chamber, which is used for different temperature requirements of different working conditions to ensure the accuracy of the experimental data.

3.2. Identification experiment

There are two methods of off-line parameter identification, one is the point calculation method and the other is the curve fitting method. The point calculation method is to draw the pulse test graph for each different SOC value and then calculate the value of each parameter at different SOC values by selecting the special points in the pulse test graph according to the formula. The other is the curve fitting method. Compared with the point-fitting method, the curve fitting method has greatly improved the utilization rate of data and is conducive to improving the accuracy of curve fitting, so the curve fitting method is chosen for parameter identification. The curve fitting method needs to give the function expression of the fitted function, which contains the parameters to be solved, input the function expression into the software, calculate the unknown quantity in the function expression according to the input expression and the existing data, and then solve for the unknown parameters to be identified in the circuit.

The open-circuit voltage, current and ohmic internal resistance can be obtained from the HPPC experiment. The zero-state response fitting curve for SOC=1 is shown in Fig. 5.

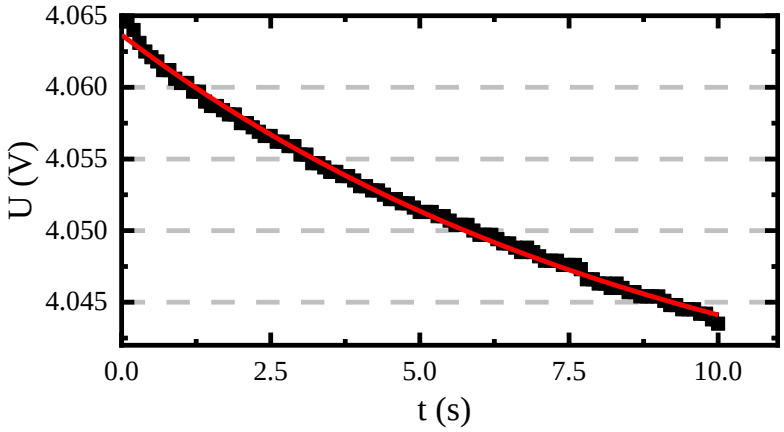

Figure 5. zero state response curve for SOC=1

The ohmic internal resistance R_0, polarized internal resistance R_p, polarized capacitance C_p, and open-circuit voltage *Uoc* are calculated for different SOC stages according to the above experimental steps as shown in Table 1.

Table 1. Model parameters under different SOC states

SOC/100%	R_0/mΩ	R_P/mΩ	*Cp*/F	*Uoc*
0.1	1.961057682	0.519082	12519.57063	3.4592
0.2	1.859498063	0.390383	19667.75322	3.5410
0.3	1.825930538	0.350388	23038.81399	3.5897
0.4	1.802504690	0.319963	23332.61905	3.6166
0.5	1.780507248	0.344103	23954.96034	3.6514
0.6	1.758224125	0.524653	16215.69966	3.7360
0.7	1.745939839	0.523653	16879.77215	3.8318
0.8	1.730370221	0.482801	17187.37110	3.9350
0.9	1.723228194	0.435092	18133.44121	4.0497
1.0	1.718942978	0.426950	22069.80251	4.1840

In the HPPC experiments, after 40 min of shelving at the end of each discharge, the battery is approximated to be in electrochemical equilibrium, i.e., the voltage at this time is the OCV value corresponding to the current SOC value. After obtaining the above data, it is possible to verify the accuracy of the selected battery model. The identified parameters are input into the Thevenin model simulated by Simulink, and the experimentally measured HPPC data are imported into the simulated Thevenin model. Fig. 5 (a) shows the voltage comparison curve, where U1 is the real voltage data from the HPPC experiment and U is the simulated voltage data from the parameters obtained by parameter

identification. The error between the simulated voltage and the real voltage data is shown in Fig. 5 (b). The error voltage is maintained at about 0.04v, and the error is less than 1%, and there is no dispersion. In the late stage of battery discharge, due to the intense chemical reaction inside the battery, the error of parameter identification increases, but in general, the error of parameter identification fluctuates within a reasonable range. The accuracy of the parameters obtained from the identification was found to be following the engineering requirements, and subsequent studies can be carried out.

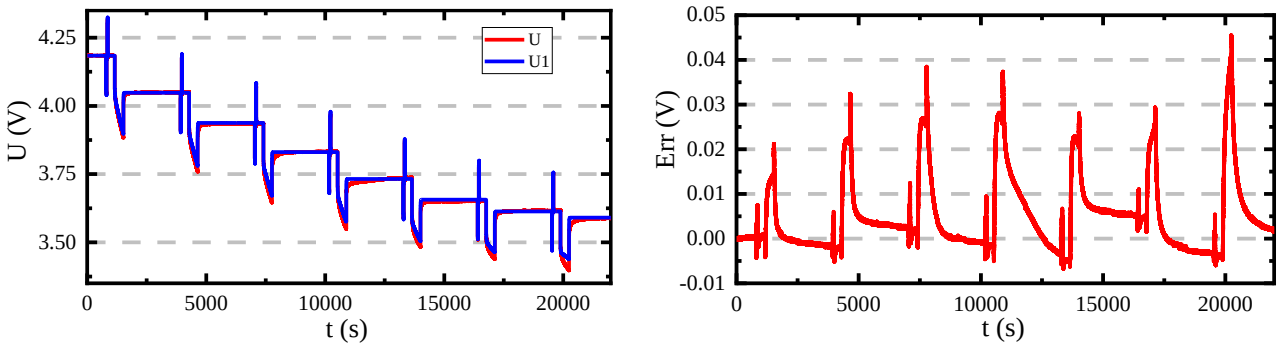

(a) Comparison of actual and simulated voltages (b) The Error of Voltage

Figure 6. Thevenin model simulation results

3.3. BBDST working condition verification

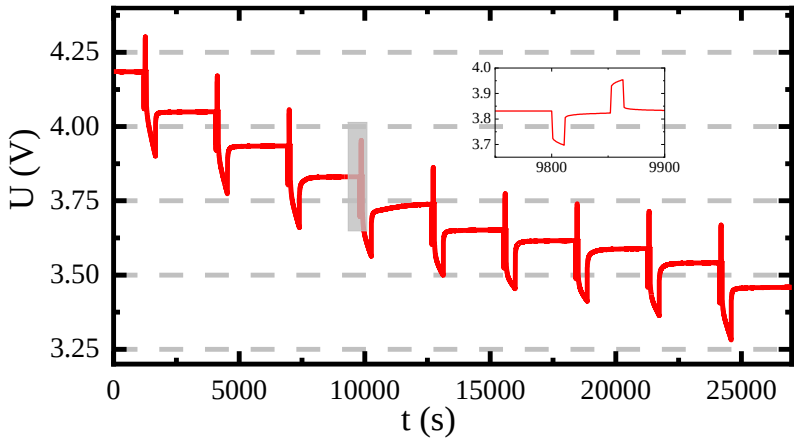

Figure 1. HPPC voltage curve

The experiment uses a Lithium-ion battery with a capacity of 70.4Ah as the modeling object, and the training model uses the data from the HPPC experiment. the HPPC sets the working condition from SOC=1 to SOC=0.1, and the sampling interval is 1s. the voltage diagram under this working condition is shown in the following Fig. 6.

The data from the HPPC experiments were input into the code written in MATLAB, and the SOC of the HPPC working condition was predicted using the CKF algorithm, and the difference between the

SOC predicted by the CKF algorithm and the result predicted by the Ansatz integral was obtained as shown in the figure below. From the results in Fig. 2, we can conclude that the experimental error results obtained by using the CKF algorithm to predict the HPPC operating conditions are basically within 0.5%, which shows that the accuracy of the SOC data predicted by using the CKF algorithm is high enough to meet the basic requirements in engineering.

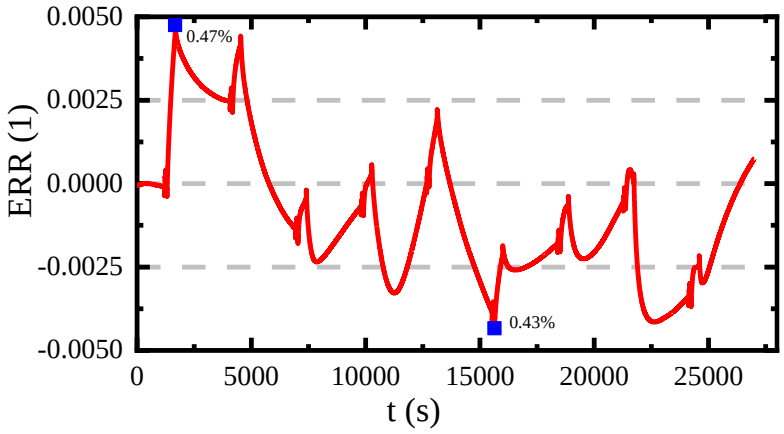

Figure 3. CKF-based Lithium-ion battery SOC estimation effect

The CKF algorithm is used to obtain the predicted SOC and end voltage errors and the voltage data under that moment into the SVM for training. 30% of the input dataset is used as training data and 70% as prediction data.

To test the accuracy of the SVM-trained model, it is validated using complex operating conditions. The data from the BBDST operating conditions were imported into the trained model, and the results and errors were compared to those predicted by the CKF-SVM algorithm, the CKF algorithm, and the ampere-time integration method, as shown in Fig. 8

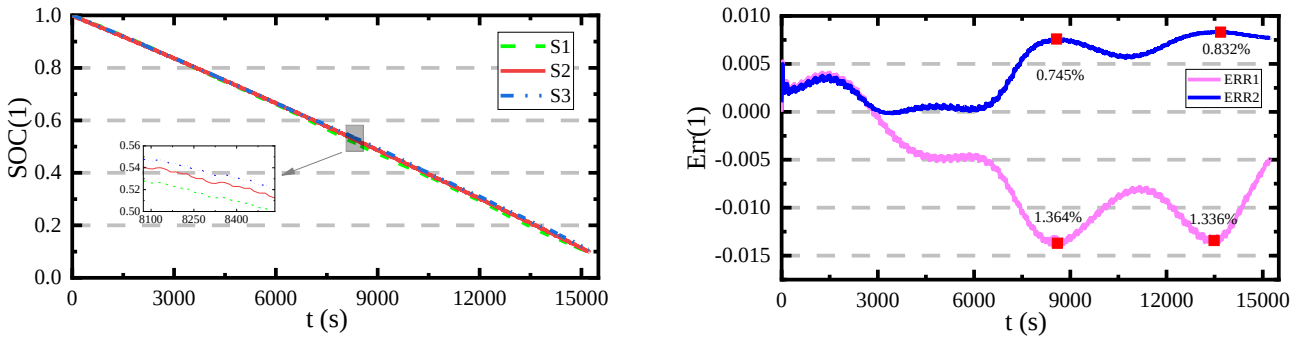

(a) SOC estimation in BBDST condition (b) SOC estimation errors in BBDST condition

Figure 4. SVM-CKF-based Lithium-ion battery SOC estimation effect in BBDST condition

In the above Fig. 7(a) S1 denotes the SOC predicted by the CKF algorithm, S2 denotes the SOC predicted by the ansatz integration method, and S3 denotes the SOC predicted by the SVM-CKF algorithm. From the above Fig. 7(a), it can be concluded that the SOC predicted by the CKF-SVM algorithm is closer to the true SOC value than the SOC predicted by the CKF algorithm. In Fig. 7(b) ERR1 is the estimation error of the CKF-SVM algorithm and ERR2 is the estimation error of the CKF algorithm. From the right figure, we can conclude that the maximum estimation error of SOC using CKF-SVM algorithm is around 0.832%, while the maximum estimation error of SOC using only CKF algorithm is around 1.364%, and we can also conclude that the estimation error of CKF-SVM algorithm fluctuates less, which reflects the good generalization ability of CKF-SVM algorithm and improves the accuracy of SOC estimation.

3.4. DST working condition verification

To avoid the accuracy of one experiment, DST working condition is predicted using the completed training model. Its SOC prediction results and prediction errors are shown in Fig. 8.

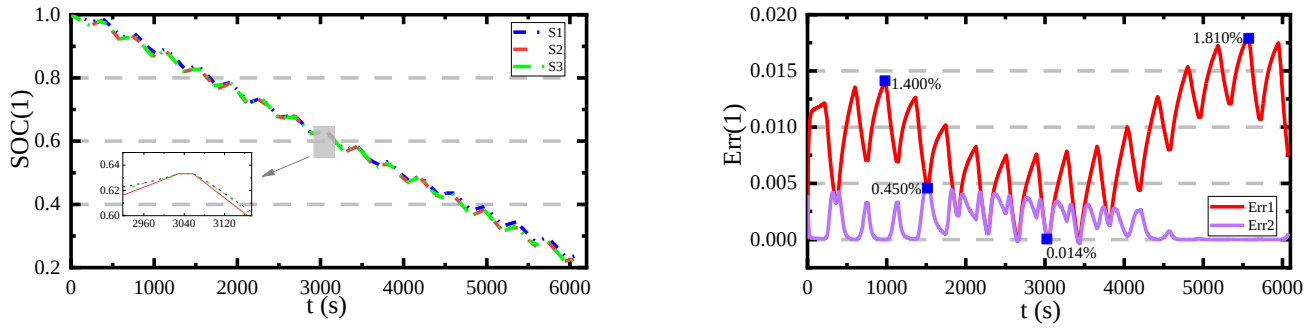

(a) SOC estimation in DST condition (b) SOC estimation error in DST condition

Figure 8. SVM-CKF-based Lithium-ion battery SOC estimation effect in DST condition

In Fig. 8(a) S1 is the SOC estimated by the CKF algorithm, S2 is the SOC estimated by the ansatz integration method, and S3 is the SOC estimated by the SVM-CKF algorithm. In Fig. 8 (b) ERR1 is the SOC estimation error of the CKF algorithm, whose maximum error is 1.81%, and ERR2 is the SOC estimation error of the SVM-CKF algorithm, whose maximum error is 0.45%. An improved neural network model and extended Kalman filter algorithm proposed in the literature [41]has a maximum error of less than 2% for SOC estimation. The maximum error of the SVM-CKF algorithm proposed in this paper for SOC estimation is less than 1%. Compared with an improved cubature Kalman algorithm[42] whose error is less than 2%, the maximum error of the SVM-CKF algorithm proposed in this paper is less than 1%, so the SVM-CKF algorithm proposed in this paper has higher accuracy. Compared with only using SVM algorithm[43], its estimation error of SOC is 6%, the error of SVM-CKF algorithm used in this paper is greatly reduced, and the error is less than 1%.

The comparison between the two can be concluded that the estimation error fluctuation of the SVM-CKF algorithm is significantly smaller than the estimation error fluctuation of the CKF algorithm, which has good generalization ability and robustness.

4. CONCLUSIONS

With the development of society and the reduction of fossil energy, the use of lithium-ion batteries will be more and more extensive. As an important factor affecting the safety and life of lithium-ion batteries, the research on SOC is also more and more extensive. This paper mainly studies the accuracy of the SVM-CKF algorithm in the prediction of lithium-ion battery SOC. In this paper, the first-order Thevenin model was constructed, and the CKF algorithm was used to predict the SOC of the HPPC experiment to obtain the input data set of the SVM algorithm. The model was obtained through SVM training, and then the model was used to compensate the SOC data predicted by the CKF algorithm under other complex working conditions to obtain more accurate SOC values. Experimental results show that the SVM-CKF algorithm can accurately estimate SOC under BBDST condition, and the maximum error of SOC estimation is 0.800%. The maximum error of the SVM-CKF algorithm in the DST condition is 0.45%. At the same time, the SVM-CKF algorithm can greatly reduce the data needed for prediction and improve the generalization ability.

ACKNOWLEDGMENTS
The work was supported by the National Natural Science Foundation of China (no. 61801407), the Sichuan Science and Technology Program (no. 2019YFG0427), the China Scholarship Council (no. 201908515099), and the Fund of Robot Technology Used for Special Environment Key Laboratory of Sichuan Province (no. 18kftk03).

References

1. D. Shindell and C. J. Smith, *Nature*, 573 (2019) 408.
2. J. E. Kay, *Nature*, 578 (2020) 45.
3. B. Pieprzyk and P. R. Hilje, *Biofuels Bioproducts & Biorefining-Biofpr*, 13 (2019) 535.
4. M. Arnaud, A. J. Baird, P. J. Morris, T. H. Dang and T. T. Nguyen, *Global Change Biology*, 26 (2020) 1899.
5. K. Nagahara, Y. Lou and E. Yanagida, *Journal of Mathematical Biology*, 82 (2021) 12.
6. Z. Huang, J. Zhu, R. J. Qiu, J. J. Ruan and R. L. Qiu, *Journal of Cleaner Production*, 229 (2019) 1148.
7. F. H. Tian, Y. J. Zhang, L. Liu, Q. Shi, J. N. Li, Q. Z. Zhao, Y. Zhang, Y. Q. Cheng, C. Zhou, S. Yang and X. P. Song, *Journal of Alloys and Compounds*, 867 (2021) 43.
8. H. H. Ryu, N. Y. Park, T. C. Noh, G. C. Kang, F. Maglia, S. J. Kim, C. S. Yoon and Y. K. Sun, *Acs Energy Letters*, 6 (2021) 216.
9. J. T. Qu, F. Liu, Y. X. Ma and J. M. Fan, *Ieee Access*, 7 (2019) 87178.
10. C. F. Pan, Y. Chen, L. M. Wang and Z. G. He, *International Journal of Electrochemical Science*, 14 (2019) 9537.
11. T. C. Ouyang, P. H. Xu, J. X. Chen, J. Lu and N. Chen, *Ieee Transactions on Power Electronics*,

36 (2021) 8102.
12. Y. Y. Jiang, J. Zhang, L. Xia and Y. B. Liu, *Ieee Access*, 8 (2020) 123858.
13. H. Ji, W. Zhang, X. H. Pan, M. Hua, Y. H. Chung, C. M. Shu and L. J. Zhang, *International Journal of Energy Research*, 44 (2020) 6502.
14. K. S. R. Mawonou, A. Eddahech, D. Dumur, D. Beauvois and E. Godoy, *Journal of Power Sources*, 484 (2021) 345.
15. T. Ould Ely, D. Kamzabek and D. Chakraborty, *Frontiers in Energy Research*, 7 (2019) 71.
16. Y. C. Fan, S. L. Wang, C. Jiang and C. Fernandez, *International Journal of Electrochemical Science*, 16 (2021) 151020.
17. Y. Q. Tan, M. J. Luo, L. Y. She and X. Y. Cui, *International Journal of Electrochemical Science*, 15 (2020) 1128.
18. K. Wang, X. Feng, J. B. Pang, J. Ren, C. X. Duan and L. W. Li, *International Journal of Electrochemical Science*, 15 (2020) 9499.
19. Z. X. Liu, Z. Li, J. B. Zhang, L. S. Su and H. Ge, *Energies*, 12 (2019) 757.
20. X. Lai, D. D. Qiao, Y. J. Zheng and L. Zhou, *Applied Sciences-Basel*, 8 (2018) 2028.
21. Z. Ren, C. Q. Du, Z. Y. Wu, J. B. Shao and W. J. Deng, *International Journal of Energy Research*, 7 (2021) 64.
22. J. P. Tian, R. Xiong, W. X. Shen and F. C. Sun, *Energy Storage Materials*, 37 (2021) 283.
23. W. H. Wang and J. Y. Mu, *Ieee Access*, 7 (2019) 29223.
24. Y. F. Liu, J. Q. Li, G. Zhang, B. Hua and N. Xiong, *Ieee Access*, 9 (2021) 34177.
25. S. Q. Li, C. K. Ju, J. L. Li, R. Fang, Z. F. Tao, B. Li and T. T. Zhang, *Energies*, 14 (2021) 306.
26. O. Ojo, H. X. Lang, Y. Kim, X. S. Hu, B. X. Mu and X. K. Lin, *Ieee Transactions on Industrial Electronics*, 68 (2021) 4068.
27. Y. Y. Liu, T. T. Cai, J. B. Liu, M. Y. Gao and Z. W. He, *Journal of Electrical Engineering & Technology*, 15 (2020) 2529.
28. Z. W. Xue, Y. Zhang, C. Cheng and G. J. Ma, *Neurocomputing*, 376 (2020) 95.
29. W. Q. Li, Y. Yang, D. Q. Wang and S. Q. Yin, *Ionics*, 26 (2020) 6145.
30. S. Yang, S. Zhou, Y. Hua, X. Zhou, X. Liu, Y. Pan, H. Ling and B. Wu, *Sci Rep*, 11 (2021) 1123.
31. Z. J. Huang, Y. S. Fang and J. J. Xu, *International Journal of Automotive Technology*, 22 (2021) 335.
32. M. Al-Gabalawy, N. S. Hosny, J. A. Dawson and A. I. Omar, *International Journal of Energy Research*, 45 (2021) 6708.
33. Y. Tian, R. Lai, X. Li, L. Xiang and J. Tian, *Applied Energy*, 265 (2020) 256.
34. Z. Liu, X. J. Dang, B. Q. Jing and J. B. Ji, *Electric Power Systems Research*, 177 (2019) 78.
35. F. Xie, S. L. Wang, Y. X. Xie, C. Fernandezb, X. X. Li and C. Y. Zou, *International Journal of Electrochemical Science*, 15 (2020) 7935.
36. L. Zhang, K. Li, D. J. Du, Y. J. Guo, M. R. Fei and Z. L. Yang, *Ieee Access*, 8 (2020) 156165.
37. X. T. Liu, X. H. Deng, Y. He, X. X. Zheng and G. J. Zeng, *Energies*, 13 (2020) 121.
38. Y. He, Q. Li, X. X. Zheng and X. T. Liu, *J. Power Electron.*, 21 (2021) 590.
39. R. Zhu, B. Duan, J. M. Zhang, Q. Zhang and C. H. Zhang, *Applied Energy*, 277 (2020) 1134.
40. Y. Tian, R. C. Lai, X. Y. Li, L. J. Xiang and J. D. Tian, *Applied Energy*, 265 (2020) 14.
41. C. Chen, R. Xiong, R. X. Yang, W. X. Shen and F. C. Sun, *Journal of Cleaner Production*, 234 (2019) 1153.
42. J. K. Peng, J. Y. Luo, H. W. He and B. Lu, *Applied Energy*, 253 (2019) 365.
43. J. C. A. Anton, P. J. G. Nieto, C. B. Viejo and J. A. V. Vilan, *Ieee Transactions on Power Electronics*, 28 (2013) 5919